Design, Development and Control of a Human-Inspired Two-Arm Robot via Pneumatic Artificial Muscles

George Andrikopoulos, *Member, IEEE* and George Nikolakopoulos

***Abstract*— In this article, the design and implementation of a 10 Degree-of-Freedom (DoF) human-inspired two-arm robot is presented. Multiple Pneumatic Artificial Muscles (PAMs) in antagonistic formations are incorporated for undertaking the two arms' movements, while the design goal is the replication of human-like motion patterns, described by smoothness, inherent compliance and accuracy. To evaluate the feasibility of the proposed concept, the 10-DoF robot is developed and experimentally tested in open and closed-loop control scenarios via the use of a multiple Advanced Nonlinear PID (ANPID) based scheme.**

I. Introduction

Muscle emulation has always been considered one of the biggest technological challenges, with the ultimate goal of creating an actuator that combines the power, accuracy and durability of mechanical drives, with the safety, controllable compliance and efficiency of biological muscles by macroscopically emulating its inherent functionality [1]. During the past few years, There has been a large research attempt in improving the design of humanoid robots via the use of inherently compliant artificial muscles [2] [3], which are characterized by flexibility and biomimetic attributes that can reproduce the smoothness, accuracy and compliance of human-inspired motion patterns [4].

This article will cover the design, development and experimental evaluation of a 10 Degree-of-Freedom (DoF) human-inspired two-arm robot, which was designed to reproduce the following human-inspired movements: a) wrist (radial/ulnar deviation), b) elbow (flexion/extension), and c) shoulder (flexion/extension, medial/lateral rotation, abduction/ adduction). The presented robotic solution will act as the mandatory infrastructure for enabling future interactive applications driven by fast, accurate, smooth and inherently safe human-inspired movements [5].

The proposed robotic setup utilizes antagonistic pairs of Pneumatic Artificial Muscles (PAMs) in order to achieve the 10 Degree-of-Freedom (DoF) movements performed via its biologically-inspired arms. This actuation method is characterized by a decrease in the actuating length when pressurized and possesses similar properties with those of the organic muscle, which include inherent compliance and high power-to-mass ratio. The PAM's expanding utilization in medical and biorobotic applications [3] is, thus, justified by its potential to cover the needs for safety, simplicity and lightness that human–robot interaction requires.

*Research funded by Innovative Arts and Science area of excellence at Luleå University of Technology and the Swedish Research Council (Vetenskaprådet).

George Andrikopoulos and George Nikolakopoulos are with the Robotics Team, Control Engineering Group, Luleå University of Technology, SE-97187 Luleå, Sweden (e-mail: {geoand, geonik} @ltu.se).

The main contribution of this article stems from the design and development of a novel robotic human-inspired setup via the utilization of PAM technology, as well as the experimental evaluation of the developed prototype's motion capabilities via the incorporation of a multiple Advanced Nonlinear PID (ANPID) control structure. The design objectives were focused on creating a human-inspired robot characterized by small weight and high motion efficiency, which acts as an alternative mechanical solution to the existing human-inspired PAM-actuated approaches in the related literature [6]–[13].

It should be noted that the presented work is based on the preliminary design presented in [14]. Following the conceptual goal of creating a human-inspired setup via PAMs, this article focuses on the following important novelties and alterations to the initial approach: a) structural redesign of the robot's joints for increased motion efficiency, b) alternative PAM placement and optimized PAM dimension selections for increased range of motion, c) experimental evaluation of the robot's capabilities via open-loop and multi-PID based control performances.

The rest of the article is structured as follows. In Section II, the design specifics of the 10-DoF human-inspired two-arm robot are presented in detail, while the motion strategy and control scheme utilized for the operation of the robot's DoFs are covered in Section III. Section IV presents the prototype development of the two-arm robot and provides an overview of the various setup components. Section V covers the experimental evaluation of the robot's capabilities in reproducing human-like movements and, finally, the concluding remarks of this work are provided in Section VI.

II. Design Specifics

The graphical representation of the two-arm humanoid robot is depicted in Fig. 1(a). The proposed biologically-inspired concept is formed on the basis of the endoskeleton proportions of an adult human, which follows an antagonistic muscle-tendon based approach for the undertaking of the robot's movements. The specific design strategy leads to a reduced-DoF solution for the replication of the following movements: a) wrist (radial/ulnar deviation), b) elbow (flexion/extension), and c) shoulder (flexion/extension, medial/lateral rotation, abduction/ adduction). In order to generate these bi-directional movements, an antagonistic PAM movement strategy is utilized, where PAMs are working antagonistically between pairs [15]. Considering the two-arm approach and the aforementioned movement patterns, the proposed design leads to a total of 10-DoFs, which are controlled by 10 respective pairs of PAMs.

A number of design challenges are imposed by the PAMs and their structural properties that need to be properly

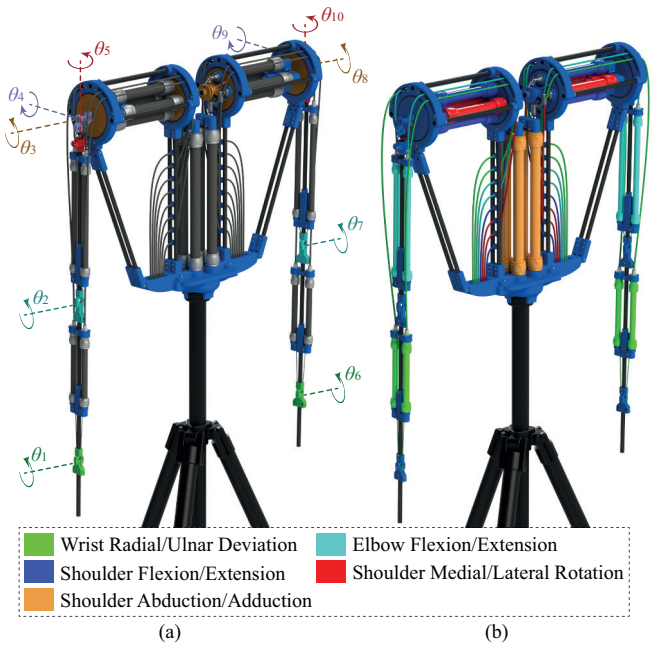

Figure 1. (a) Conceptual design of the human-inspired two-arm robot with color highlighed revolute joints accompanied by the respective target movements, (b) color-highlighted antagonistical pairs of PAMs, tendons and pneumatic tubes.

addressed. Specifically, the PAM technology provides a maximum of 30% permissible stroke, compared to the 50-70% of the biological muscle [16], while the forces exerted on the PAMs during movement have a direct impact on their permissible contraction [17], [18].

In order to alleviate the effect of these properties and increase the motion efficiency of the proposed robot, a number of design guidelines is followed: a) the placement of each PAM pair is properly selected in order to simplify the complexity of the various movement scenarios, when compared to the synergistic and highly coupled nature of the biological muscles [5], b) the design follows a trade-off between joint angle and torque by incorporating a biomimetic muscle-tendon strategy, where tendon-like strings utilized to transfer the PAM linear motion to the joints, c) a structural support is utilized in order to ensure the linear motion of the elastic PAMs and avoid any loss in effective contraction due to non-axial bending motions, and d) an optimized design strategy is followed on the pneumatic tube handling, in order to minimize any additional tension during motion.

The utilized antagonistic PAM pairs, the respective tendon-like strings and the selected pneumatic tube handling strategy are depicted in Fig. 1(b), while accompanied by color-matched information to the respective movements. The respective joints incorporated in the robotic structure for the reproduction of the target movements are revolute in design and are presented in Fig. 1(a), where θ denotes the angular motion of the i-th joint for i = 1,…,10. Note that joints i = 1,…,5 and i = 6,…10 correspond to the PAM pairs used in the two symmetrical arms, respectively.

Exploded views of the utilized joints are displayed in Fig. 2. The presented details highlight the use of bearing-based approach for achieving maximum joint smoothness, while the strategy for converting the PAMs' linear displacement to

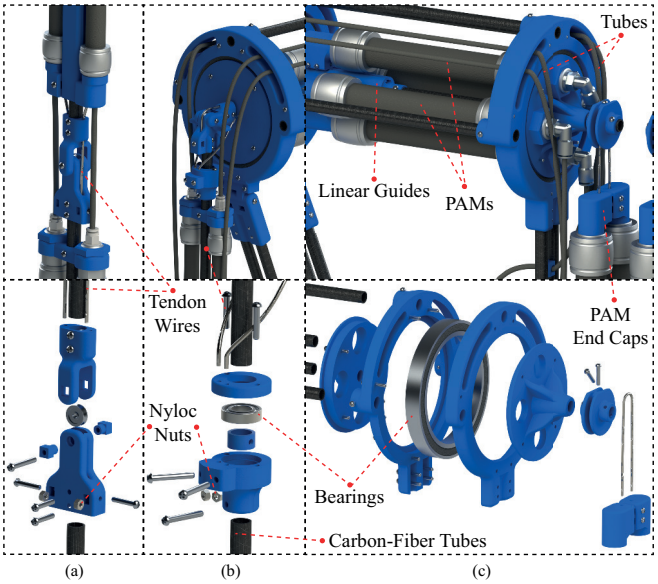

Figure 2. Design details in assembled (top) and exploded view (bottom) for the (a) elbow and (b-c) shoulder joints.

angular movement can also be observed, with all tendons being attached to the PAMs' end cap parts and to the respective point of rotation. The utilized strategy is focused on a rapid prototyping-friendly approach, with appropriate inlets on the endoskeleton structure to guide the tendons' movement and ensure smoothness and efficiency, while incorporating Nyloc nuts for their tight attachment to the PAM end caps and their respective end-points. It has to be noted that the wrist, elbow and shoulder (abduction/adduction) joints are of the same structure, hence the inclusion of only the elbow joint in Fig. 2(a).

For the replication of the shoulder's 3-DoFs, three rotation joints are combined, as shown in Fig. 2(b-c). The PAMs involved in the shoulder's medial/lateral rotation and abduction/adduction are placed on a rotatable endoskeletal area, rather than the space around the back and abdomen. This novel strategy includes the use of eccentric tendon connections for the shoulder medial-lateral rotation, which force a planar motion transfer from the PAMs to the successful rotational movement of the joint. Furthermore, the shoulder flexion/extension is generated via a vertically positioned pair of PAMs in the sternum area, which ultimately controls the rotation of the endoskeletal shoulder formation and while being placed close to the structure in order to minimize the effect of their pulling tension. In this way, the shoulder's 3-DoFs can now be performed independently of the shoulder rotation state.

III. Motion Strategy and Control Scheme

A. Motion Strategy

The utilized motion strategy has the PAMs connected to their respective tendons, while initially inflated at an initial pressure P_0 that corresponds to the half of their maximum permissible stroke. In this way, the full PAM stroke is utilized that leads to the maximum provided range of motion for every DoF. With that in mind, the antagonistic movement strategy is formulated in (1), where $P_{i,j}$ defines the pressure values utilized in every antagonistic pair of PAMs, identified as j = 1,2, for the undertaking of the i = 1,…,10 joint

movements described in the previous Subsection, while $P_{i,0}$ denotes the initial pressure of the i-th PAM pair. This strategy has the advantage of utilizing one manipulated pressure variable ΔP_i that is being respectively added and subtracted from the antagonistic PAM pair and depending on its sign causes the desired motion pattern.

$$P_{i,j} = P_{i,0} \pm \Delta P_i \text{ for } \begin{cases} i=1,6 \Rightarrow \begin{cases} \text{Wrist Radial Deviation } (\Delta P_i > 0) \\ \text{Wrist Ulnar Deviation } (\Delta P_i < 0) \end{cases} \\ i=2,7 \Rightarrow \begin{cases} \text{Elbow Flexion } (\Delta P_i > 0) \\ \text{Elbow Extension } (\Delta P_i < 0) \end{cases} \\ i=3,8 \Rightarrow \begin{cases} \text{Shoulder Flexion } (\Delta P_i > 0) \\ \text{Shoulder Extension } (\Delta P_i < 0) \end{cases} \\ i=4,9 \Rightarrow \begin{cases} \text{Shoulder Abduction } (\Delta P_i > 0) \\ \text{Shoulder Adduction } (\Delta P_i < 0) \end{cases} \\ i=5,10 \Rightarrow \begin{cases} \text{Shoulder Medial Rotation } (\Delta P_i > 0) \\ \text{Shoulder Lateral Rotation } (\Delta P_i < 0) \end{cases} \end{cases} \quad (1)$$

To address the system's mechanical coupling on the shoulder's four PAM formation utilized for the Abduction/Adduction and Flexion/Extension, the motion law of (1) is modified as shown below:

$$P_{i,j} = aP_{i,0} \pm \Delta P_i, \text{ for } i = 4,9 \quad (2)$$

where $a \in [0,1]$ is a function of $P_{I,j}$ for i = 3,8. This modified strategy is used for ensuring a limited mechanical stress on the affected joints when the two aforementioned shoulder movements are performed simultaneously.

B. Control Structure

For the preliminary evaluation of the proposed setup's motion capabilities, the ANPID algorithm is utilized due to its increased flexibility and adaptability, as well as its experimentally verified capability in producing smooth, fast and accurate PAM responses [17]. It has to be noted that this preliminary evaluation concerns the angular control of the robot's joints, while the synthesis of torque and compliance controllers is part of future work. Given the movement strategy described in (1), the robot's motion control problem is addressed via the use of a multiple ANPID-based control structure under the assumption of a sampling process with a sampling period $T_s \in \mathbb{R}^+$, while at sample $n \in \mathbb{Z}^+$. Compared to the standard PID structure [19], which utilizes a proportional gain K_P, a reset time T_I and a rate time T_D, the ANPID structure incorporates additional control parameters which synthesize the following modified error signals e_P, e_I and e_D for the proportional, integral and derivative control action terms, respectively:

$$\begin{aligned} e_P(n) &= \frac{\left[f x_{\text{ref}}(n) - x(n)\right]}{x_{\text{ref,range}}}\left[g x_{\text{ref,range}} + (1-g)\left|f x_{\text{ref}}(n) - x(n)\right|\right], \\ e_I(n) &= \frac{\left[x_{\text{ref}}(n) - x(n)\right]}{x_{\text{ref,range}}}\left[g x_{\text{ref,range}} + (1-g)\left|x_{\text{ref}}(n) - x(n)\right|\right], \\ e_D(n) &= \frac{\left[q x_{\text{ref}}(n) - x(n)\right]}{x_{\text{ref,range}}}\left[g x_{\text{ref,range}} + (1-g)\left|q x_{\text{ref}}(n) - x(n)\right|\right]. \end{aligned} \quad (3)$$

where $x_{\text{ref,range}}$ denotes the range of the reference output x. The mode selector $f \in [0,1]$ is utilized as a relative trade-off between noise rejection and set-point tracking, $q \in [0,1]$ accounts for differentiation on error (q=1) or measurement (q=0) and $g \in [0,1]$, is properly introduced in (2) to achieve an adjustable decrease of K_p gain at low error magnitudes and the corresponding gradual increase at large deviations from the set-point. Thus, the discrete time control action $u(n)$ of the ANPID algorithm is being formulated as shown below:

$$u(n) = K_P\left[e_P(n) + \delta\frac{T_s}{T_I}\sum_{i=1}^{n}\left[\frac{e_I(i) + e_I(i-1)}{2}\right]h(i) + \frac{T_D}{T_s}\left[e_D(n) - e_D(n-1)\right]\right]. \quad (4)$$

where $h(n) = \left(\frac{x_{\text{ref,range}}^2}{x_{\text{ref,range}}^2 + 10e_I^2(n)}\right)$ defines the discrete representation utilized for the nonlinear adjustment of the internal term in order to counteract overshoot phenomena. In addition, a switch function δ that is defined in (5):

$$\delta = \begin{cases} 1 & \text{for } u_{\min} \le u(n) \le u_{\max} \\ 0 & \text{if } u(n) \le u_{\min} \text{ or } u(n) \ge u_{\max} \end{cases}, \quad (5)$$

is incorporated in the integral control action of (4) to avoid the intense overshoot phenomena that follow cases of a constant error factor, where the integral action drives the control effort to its extreme values $u_{\min}$ or $u_{\max}$, resulting in a saturated condition called "wind-up".

In this case, ten ANPID algorithms are utilized for the control of the ten respective DoFs of the two-arm robot. Specifically, in each ANPID the manipulated variable u responds to the pressure ΔP_i presented in (1), the process value x is the resulting angular motion θ_i of the i-th joint, while the mode selectors are respectively defined as f_i, q_i, and g_i. Thus, the following error definition is formulated:

$$e_i = \theta_{i,\text{ref}} - \theta_i \quad (6)$$

where the subscript $(\cdot)_{\text{i,ref}}$ denotes the respective reference angle values. Further analysis of the utilized control scheme's properties is provided in [17].

IV. Prototype Development and Setup Components

A. Prototype Development

A 10-DoF two-arm robot prototype was developed by following the design specifics described in Section II and is presented in Fig. 3, where the basic components forming its skeletal structure are properly highlighted. The prototype followed the dimensions of an adult male proportionally scaled up by 20 %. Characteristically, the shoulder-to-shoulder distance was implemented at 0.67 m, the arm length at 0.94 m, while the span of the robot's reach when the arms were fully abducted was noted at 2.55 m.

Following the selected dimensions, for the reproduction of the 10-DoFs twenty FESTO Fluidic Muscles of different internal diameters and nominal lengths were utilized, of which: a) four DMSP-10-120N-AM-CM with 10 mm internal nominal diameter and 120 mm nominal length for the wrists, b) four DMSP-10-214N-AM-CM with 10 mm internal diameter and 214 mm nominal length for the elbows, c) eight DMSP-20-120N-AM-CM with 20 mm internal nominal diameter and 120 mm nominal length for the shoulder abduction/adduction and flexion/extension, and d) four DMSP-20-260N-AM-CM with 20 mm internal nominal

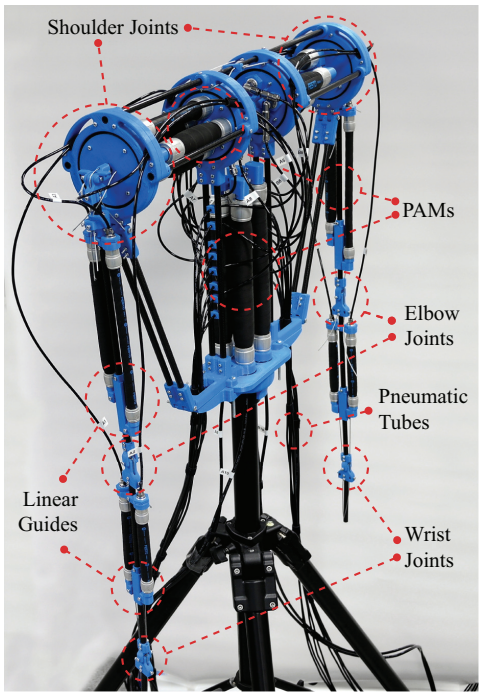

Figure 3. The two-arm humanoid robot prototype.

diameter and 260 mm for the shoulder medial/lateral rotation. The nominal length and internal diameters of the PAMs has been selected by taking into consideration the dimension proportional restrictions of the biomimetic design and the estimated motion properties extracted via simulation studies.

In order to minimize the inertial effects of the arm's equipment during joint motion, as well as to increase the overall motion efficiency and the achieved workspace, low-weight materials were utilized in the construction of the skeletal setup. Specifically and as shown in Fig. 3, carbon-fiber tubes were used in the skeleton to provide increased durability, while the various joint parts, linear guides, tube enclosures and connection components have being 3D printed via PLA material. The 3D printed parts undergoing contact and relative movement during the robot's operation, such as the linear guides and the tubing covers, were properly prepped and processed in order to minimize friction.

Finally, 2 mm steel wire was selected for the role of the artificial tendons and deep groove ball bearings were incorporated in the joint mechanisms for increased motion sensitivity and smoothness. The above selection of materials led to a two-arm robot that weighs approximately 7.32 kg, of which 3.35 kg belong to the utilized PAMs. To the author's best knowledge, this is one of the smallest documented weights in related bibliography regarding a two-arm humanoid design of these dimensions [1], [2].

B. Setup Components

The control and pressure measurement of the compressed air supplied into the PAMs was achieved via twenty FESTO VPPM-6F-L-1-F-0L10H-V1N-S1 proportional pressure regulators. The utilized pressure sensors, which are integrated inside the aforementioned pressure regulators, provide a measurement accuracy of ±0.0035 bar. Moreover, a VICON motion capturing system consisted of twenty IR cameras was

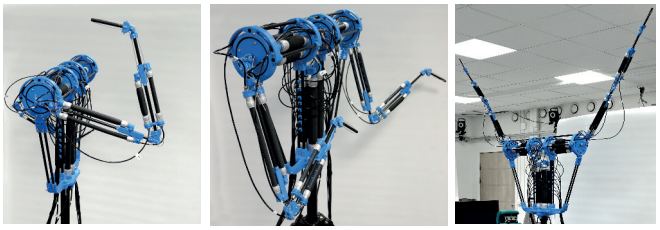

(a) (b) (c)

Figure 4. Photographic stills of the humanoid's performance taken during random motion scenarios involving: (a) wrist radial deviation, elbow flexion and shoulder flexion/extention, (b) wrist ulnar deviation, elbow flexion and shoulder medial/lateral rotation, and (c) shoulder abduction.

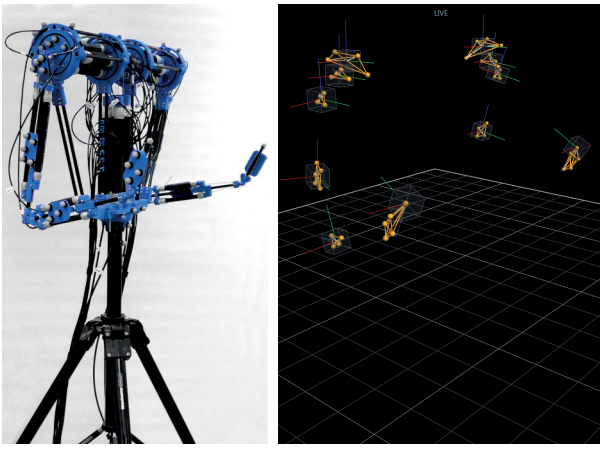

Figure 5. The humanoid arm setup equipped with marker-defined objects (left) and the captured reconstructed model via the VICON system (right).

utilized for the measurement and acquisition of the angular and translational motion data, which provides a high sensing translation accuracy of approximately 0.04 mm and a respective angular accuracy of 0.02 degrees. Finally, the control of the setup's operation, as well as the data acquisition, were achieved via two USB-1608G and two USB-3100 data acquisition cards supplied by Measurement Computing, while the setup's programming software has been developed in National Instruments LabVIEW.

V. Experimental Evaluation

In this section, the experimental results regarding the evaluation of the two-arm prototype's motion capabilities are presented. Multiple experimental sequences were executed in order to assess the setup's 10-DoF motions and its ability in reproducing human-like movements through its biomimetic wrists, elbows and shoulders. It has to be noted that throughout the presented trials, all pressure signals, which were calculated via (1) via the appropriate change of the pressure element ΔP_i, were constrained to the PAM's permissible range $0 \leq P_{i,j} \leq 8$ bar.

Initially, experimental trials concerning open-loop responses were performed in order to test all possible movement patterns of the humanoid arms. Fig. 4 presents photographic stills taken during random motion sequences, which produce a human-like optical result.

In the sequel, the translational and angular data of every joint were acquired via the VICON motion capturing system, as graphically presented in Fig. 5. Table I presents the

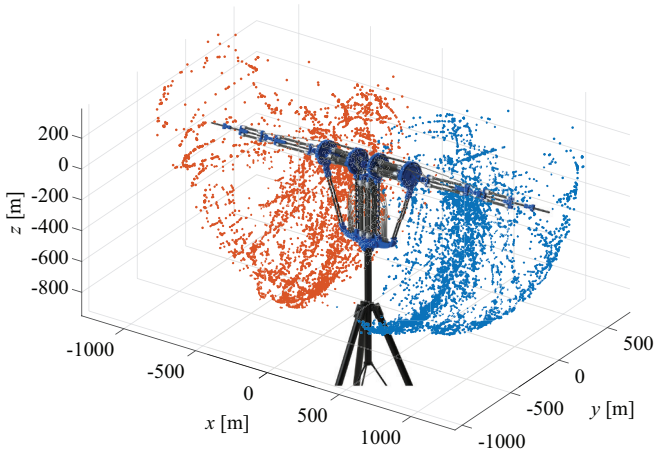

Figure 6. The experimentally acquired workspace of the two-arm humanoid prototype, where red and blue coloring highlights the workspace of the left and right arm, respectively.

TABLE I. TWO-ARM ROBOTIC PROTOTYPE'S RANGE OF MOTIONS

i	$P_{0,i}$ [bar]	Movement Type		Maximum Angle [deg]
1,6	3.81	Wrist	Radial Deviation	71.6
			Ulnar Deviation	70.4
2,7	3.62	Elbow	Flexion	111.4
			Extension	3.2
3,8	3.91	Shoulder	Flexion	71.05
			Extension	65.8
4,9	3.40		Abduction	147.6
			Adduction	10.5
5,10	3.21		Medial Rotation	82.4
			Lateral Rotation	60.2

acquired maximum angular range of the prototype's, with respect to the idle state depicted in Fig. 3, along with the utilized initial pressures $P_{0,i}$. It has to be noted that the elbow's extension is close to 3 degrees, a motion property adjusted in order to agree with the human elbow's very small extension capability. Similarly, the maximum elbow flexion and shoulder adduction were constrained to the presented values, in order to avoid the collision of the arms' components with the rest of the endoskeletal parts.

The repetition of the open-loop motion experiments for all joint combinations and the acquisition of the two arm's end-effectors resulted in the total reachable workspace presented in Fig. 6. The acquired result reveals the extensive workspace of the proposed design, while being characterized by ranges of motion comparable to those of an adult male.

Following the open-loop experimental evaluation, the proposed ANPID-based structure undertakes the angular control of the robotic prototype's 10 DoFs. For these experiments, the ANPID mode selectors were empirically adjusted at $f = 0.75$ and $q = 0$, leading to a linearly adjustable proportional action for balanced disturbance rejection and set-point tracking, along with a measurement-affected derivative action for reduced derivative kick effect in cases of sudden set-point alterations. The linearity factor g was set to $g = 0.81$, in order to achieve a smooth non-linear adjustment of the error signal and a decrease of the K_p gain at low error

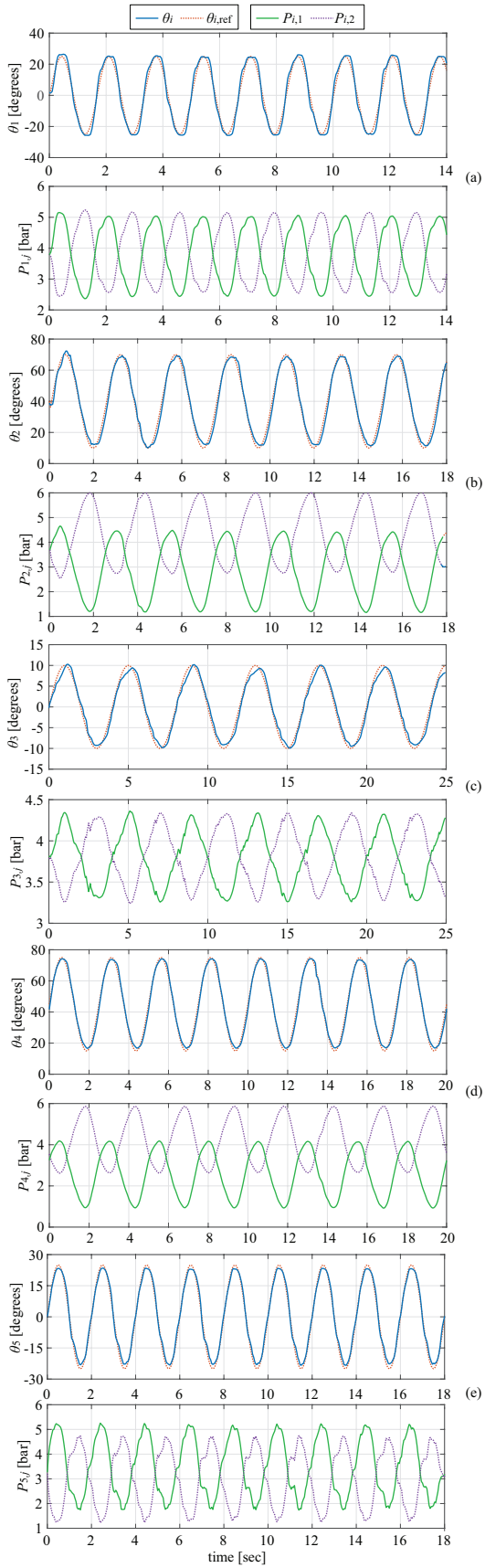

Figure 7. Angular responses of the ANPID-based structure during the prototype's performance of (a) wrist radial/ulnar deviation, (b) elbow flexion/extension, and shoulder (c) flexion/extension, (d) abduction/adduction and (e) medial/lateral rotation.

magnitudes. Finally, the control parameters K_P, T_I and T_D are fine-tuned through extensive experimental trials.

Experimental sequences were performed for the preliminary evaluation of the closed-loop system's ability to track challenging reference signals in terms of range and frequency. Specifically, the angular responses θ_i for i = 1,…,5, as defined in (1), and sinusoidal reference signals of different ranges and frequencies are depicted in Fig. 7, along with their respective pressure control efforts $P_{i,j}$. It has to be noted that the presented results were of identical properties for both arms, hence the inclusion of only one arm responses for simplification purposes.

The multiple ANPID-based scheme manages to track all reference signals performance, while the same control quality is maintained for all target movements. The system provides smooth tracking despite the selected angular reference inputs, which cover a large part of the robot's operational range, as well as the frequency of the reference signals by taking into account the inherently large settling times of the utilized PAMs. The mean absolute errors calculated for the presented experiments remain at low values and are measured below 0.69^o for all cases. It has to be noted that the same control performance is also maintained for higher frequencies, with the evaluation of the two-arm robot's performance in such challenging scenarios being a part of ongoing work.

VI. Conclusions

In this article, the conceptual design of a 10 DoF human-inspired two-arm robot was presented, with the goal of producing a setup actuated via Pneumatic Artificial Muscles (PAMs) and able to reproduce the following arm movements: (a) wrist radial/ulnar deviation, (b) elbow flexion/extension, and shoulder (c) flexion/extension, (d) abduction/adduction and (e) medial/lateral rotation. The design specifics of the proposed robot were presented in detail, by giving emphasis on the antagonistic configuration and placement of the PAMs into the endoskeleton concept.

For the evaluation of the conceptual design, a two-arm robot prototype was developed and its motion capabilities were evaluated via open and closed-loop sequences. The results of a preliminary open-loop evaluation showed that the setup can produce an extensive workspace with arm motion ranges comparable to those of the human arm, while producing human-like postures. Experimental sequences via the incorporation of a control scheme involving multiple Advance Nonlinear PID (ANPID) controllers showed that this robotic solution manages to track reference signals of high range and frequency in a smooth, fast and accurate manner. In overall, the experimental evaluation revealed that this novel endoskeletal design possesses the structural attributes necessary for biomimetic reproduction of the basic movements of the human arms, thus enabling the expansion of this concept towards a full-body configuration.

The authors have to note that the presented research concerned the evaluation of the two-arm robot prototype, where the reduced-DoF approach was considered as a basic motion problem. The evaluation of more complex schemes for simultaneous position and compliance control for safe human-robot interaction are part of future work.

Acknowledgments

The authors would like to express their gratitude to Prof. Åsa Unander-Scharin and Dariusz Kominiak for their valuable insight on the conceptual design of the proposed two-arm robot. They would also like to thank Anna Costalonga for her help in performing the experimental evaluation sequences.

References

[1] H. Inoue "Whither Robotics: Key Issues, Approaches and Applications", IROS'96, Osaka, Japan, 1996, p. 9–14.

[2] J. Wang, "A survey on the structures of current mobile humanoid robots", in Proc. of *IEEE Asia Pacific Conference on Circuits and Systems* (APCCAS), 30 Nov. - 3 Dec., 2008, Macao.

[3] G. Andrikopoulos, G. Nikolakopoulos, and S. Manesis, "A Survey on applications of Pneumatic Artificial Muscles," in *Mediterranean Conference on Control and Automation (MED)*, 2011, pp. 1439-1446.

[4] G. A. Bekey, "Robotics: State of the Art and Future Challanges," Imperial College Press, 2008.

[5] R. Drake, "Gray's Anatomy for Students", Third Edition, Elsevier, 2015.

[6] J. Schröder, K. Kawamura, T. Gockel, and R. Dillmann, "Improved Control of a Humanoid Arm Driven by Pneumatic Actuators," in *International Conference on Humanoid Robots*, 2003, pp. 1–20.

[7] D. Shin, I. Sardellitti, and O. Khatib., "A hybrid actuation approach for human-friendly robot design," in Proc. of the *2008 IEEE International Conference on Robotics and Automation* (ICRA), 2008.

[8] G. K. Hari, S. Lal, B. Tondu, J. Manhes, O. Stasse, and P. Soueres, "Performing Explosive motions using a multi-joint arm actuated by pneumatic muscles with quasi-DDP optimal control," in *IEEE Multi-Conference on Systems and Control* (MSC), 2016, no. 1.

[9] I. Boblan and A. Schulz, "A Humanoid Muscle Robot Torso with Biologically Inspired Construction," *in ISR 2010, 41st International Symposium on Robotics and ROBOTIK 2010*, 6th German Conference on Robotics, Munich, Germany, 2010.

[10] P. Kormushev, D. N. Nenchev, S. Calinon, and D. G. Caldwell, "Upper-body kinesthetic teaching of a free-standing humanoid robot,", in Proc. of *IEEE International Conference on Robotics and Automation* (ICRA), 9-13 May, 2011, Shanghai.

[11] K. Kawashima, T. Sasaki, T. Miyata, N. Nakamura, M. Sekiguchi, and T. Kagawa, "Development of robot using pneumatic artificial rubber muscles to operate construction machinery," *J. Robotics and Mechatronics*, vol. 16, no. 1, pp. 8–15, 2004.

[12] RoboThespian, Engineered Arts Limited (Penryn, Cornwall, U.K. 2010).

[13] C. Borst, C. Ott, T. Wimbock, and B. Brunner, "A humanoid upper body system for two-handed manipulation," in *IEEE International Conference on Robotics and Automation* (ICRA), 10-14 April, 2007, Roma, Italy.

[14] G. Andrikopoulos, G. Nikolakopoulos, D. Kominiak, and Å. Unander-Scharin, "Towards the Development of a Novel Upper-Body Pneumatic Humanoid: Design and Implementation," in *European Control Conference* (ECC), 29 June - 1 July, 2016, Aalborg, Denmark.

[15] B. Tondu and P. Lopez, "Modeling and control of McKibben artificial muscle robot actuators," *IEEE Control Systems Magazine*, vol. 20, no. 2, pp. 15–38, 2000.

[16] R. Dillmann, "Künstliche Muskeln als optimale", Antriebe, Institut für technische Informatik, Universität Karlsruhe.

[17] G. Andrikopoulos, G. Nikolakopoulos, and S. Manesis, "Advanced Non-linear PID Based Antagonistic Control for Pneumatic Muscle Actuators", in *IEEE Transactions on Industrial Electronics* (TIE), vol. 61, no. 12, pp. 6926 – 6937, December 2014.

[18] G. Andrikopoulos, G. Nikolakopoulos, and S. Manesis, "Adaptive Internal Model Control Scheme for a Pneumatic Artificial Muscle", in European Control Conference (ECC), 17-19 July 2013, pp. 772-777, Zurich, Switzerland.

[19] K. J. Åström, and T. Hagglund, "PID Controllers: Theory, Design and Tuning", Instrument Society of America, pp. 343, 1995.